ELSEVIER

Factors influencing encapsulation behavior in composite droplet-type polymer blends

Joël Reignier, Basil D. Favis*, Marie-Claude Heuzey

CRASP, Department of Chemical Engineering, Ecole Polytechnique, P.O. Box 6079, Station Centre-Ville, Montreal, Que., Canada H3C 3A7

Abstract

In this study the influence of the molecular weight of the dispersed phase components on encapsulation effects in the composite droplet phase was examined for high density polyethylene (HDPE)/PS/PMMA ternary blends. Three different blends composed of various PS and PMMA materials dispersed in an HDPE matrix were prepared using an internal mixer. The morphology was studied by light and electron microscopy. Current models used for predicting encapsulation effects and composite droplet formation in ternary systems (based on static interfacial tension) predict in all cases that PS will encapsulate the PMMA. However, in one case, an unexpected encapsulation of PS by PMMA was observed. It was found that arguments based on the effect of viscosity ratio or the absolute viscosity of the different dispersed phases do not explain that discrepancy. In addition, the reversal of that latter composite droplet morphology from PMMA encapsulating PS to PS encapsulating PMMA was observed upon annealing treatment. Considering all the above, a conceptual model was developed to predict encapsulation effects in composite droplet type systems based on the use of a dynamic interfacial tension (i.e. taking into account the elasticity of the polymer components). Calculations based on the dynamic interfacial tension model, using elasticities based on constant shear stress, were able to account for all of the observed encapsulation effects in this study.
© 2002 Elsevier Science Ltd. All rights reserved.

Keywords: Composite-droplet; Encapsulation; Viscoelasticity

1. Introduction

The vast majority of the polymer blend literature is related to the study of a pure dispersed phase in matrix system. Recently, there has been interest in another structure, the composite droplet morphology. The term, composite droplet, is used to specifically describe the case of a dispersed phase which contains subinclusions. The existence of such structures have been known for some time in emulsion systems [1]. Their study using as-polymerized components is of great potential since they indicate a possible route towards next generation polymer blends where the dispersed phase itself can be controlled as a discrete polymer blend. This approach should clearly allow for a more sophisticated control over the final physical properties of the blend material.

Favis and Chalifoux [2] showed that a composite droplet structure could be generated for a 50/50% incompatible binary blend of polypropylene (PP) and polycarbonate (PC) during melt blending near the phase inversion region. They

also achieved this structure [3] at lower PC concentration (25 vol%) by selectively imposing phase inversion and controlling the time of mixing. That system consisted of a PP matrix and PP subinclusions within the more viscous PC dispersed phase. Increasing the viscosity of the dispersed phase was found to improve the retention of subinclusions with mixing time. By imposing interfacial interactions between the subinclusions and the dispersed phase they were able to achieve highly stable composite droplet morphologies.

In studies of multicomponent polymer blends of more than two phases, papers dedicated to this subject showed that the morphology resulting from the blending process depends mainly upon the interfacial properties of the molten components. Hobbs et al. [4] first reported on the spontaneous development of the composite droplet morphology in immiscible as-polymerized systems using melt processing equipment. They suggested that under equilibrium mixing conditions, interfacial forces might play an important role in establishing the phase morphology of multiphase polymer blends. By using the concept of a spreading coefficient, they rewrote the Harkin's equation in

---

* Corresponding author. Tel.: +1-514-340-4629; fax: +1-514-340-2994.
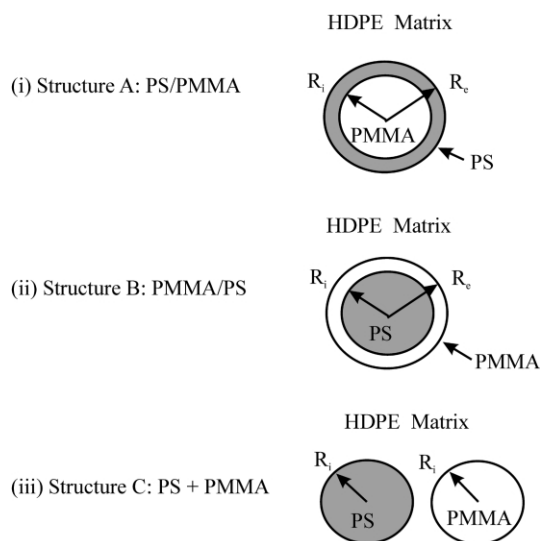
Fig. 1. Schematic illustrations showing the three possible structures for a ternary blend with a HDPE matrix: (i) the PMMA phase is encapsulated by the PS phase (PS/PMMA); (ii) the PS phase is encapsulated by the PMMA phase (PMMA/PS); (iii) PS and PMMA dispersed phases remain separate (PS + PMMA). Only structures A and B are observed in this work.

which two dissimilar phases are dispersed within a third matrix material by substituting the appropriate interfacial tensions for the surface tension values

$$\lambda_{31} = \sigma_{12} - \sigma_{32} - \sigma_{13} \qquad (1)$$

where σ_{12}, σ_{32} and σ_{13} are the interfacial tensions for each component pair, and λ_{31} is defined as the spreading coefficient for the case of component 3 encapsulating component 1 [4]. The index 2 refers to the matrix. λ_{31} must be positive for component 1 to be encapsulated by component 3. They successfully demonstrated the usefulness of the spreading coefficient concept to predict the various morphologies which were formed, and in particular the encapsulation effect.

Guo et al. [5] extended the concept of the spreading coefficient to take into account the overall surface free energy by including the interfacial area of each component. They developed Eq. (2) which states that the equilibrium phase structure of a multiphase system is determined by the lowest free energy state defined by

$$G = \sum_i n_i \mu_i + \sum_{i \neq j} A_i \sigma_{ij} \qquad (2)$$

where G is the Gibbs free energy; n, the number of moles; μ, the chemical potential; A, the interfacial area and σ is the interfacial tension. Fig. 1 shows the three possible phase structures for a ternary blend where high density polyethylene (HDPE) is the matrix phase and PS and PMMA are the dispersed phases: (i) the PMMA phase is encapsulated by the PS phase (PS/PMMA); (ii) the PS phase is encapsulated by the PMMA phase (PMMA/PS); and (iii) the PS and PMMA phases form separate phases (PS + PMMA). The morphology of the ternary polymer blend can

be predicted by comparing the interfacial free energy of the different structures. Calculations based on Eq. (2) demonstrate that the model predicts that the interfacial tension plays the major role in establishing the phase structure, whereas a less significant role is played by the surface area of the dispersed phases. The morphology obtained for different HDPE/PP/PS and HDPE/PMMA/PS ternary systems agree with those predicted by the model [5].

It is possible to control encapsulation behavior by changing the interfacial tension of a specific polymer pair in the ternary blend [5,6]. Legros et al. [6] reported on a morphological study of poly(butylene-terephtalate) (PBT)/ polyethylene (PE)/ethylene vinyl acetate (EVA) ternary blends. This system demonstrates very little subinclusion behavior. However, after addition of a transesterification precursor (Bu$_2$SnO), which is a selective interfacial modifier for PBT/EVA, the blend forms a composite droplet morphology with EVA encapsulating PE. The in situ formation of PBT/EVA copolymer, results in an interfacial tension reduction between the PBT and the EVA, leading to a much more positive EVA/PE spreading coefficient. Guo et al. [5] showed the reverse effect and demonstrated that the phase structure of a HDPE/PP/PS ternary system (with HDPE as the matrix component) changed from a composite droplet structure of PS engulfed by PP to separate droplets by the addition to the blend system of a small amount of an interfacial modifier poly(styrene-b-ethylene) (S–E) block copolymer. The reduction in the PS/HDPE interfacial tension reduced the spreading coefficient $\lambda_{PP/PS}$ to a negative value.

Recent papers on ternary systems have suggested that composite droplet formation may be related to the viscosity of the dispersed components. Nemirovski et al. [7] studied the phase morphology of a number of three-component (thermoplastic/thermotropic) systems and suggested that the dispersed component A will encapsulate the dispersed component B (in a matrix C) when both the thermodynamics, expressed by means of a positive $\lambda_{A/B}$ spreading coefficient, and kinetic effects, expressed by means of η_A/η_B dispersed phase viscosity ratio smaller than 1, act cooperatively. However, in some cases, a dispersed phase viscosity ratio η_A/η_B greater than 1 was found to hinder the development of the core–shell structure (A encapsulating B) even though encapsulation had been predicted by a positive $\lambda_{A/B}$ spreading coefficient. The reverse effect was observed by Gupta and Srinivasan [8] for ternary blends of styrene–ethylene–butylene terpolymer (SEBS) and polycarbonate (PC) dispersed within a PP matrix. The SEBS component forms a boundary layer at the surface of the PC droplets when PC is less viscous than SEBS, whereas the minor components are separately dispersed when PC is more viscous than SEBS. However, most authors have not found any influence of the dispersed phase core–shell viscosity ratio on the composite droplet structure [9,10]. Hemmati et al. [9] showed for various ternary blends of 70/ 15/15 PP/rubber/HDPE that changing the rubber/HDPE

torque ratio from 0.86 to 100 has no effect on the morphology; in all cases the HDPE component is encapsulated by the rubber phase, in agreement with the theoretical prediction based on the spreading coefficient. Work done by Luzinov et al. [10] on ternary blends consisting of polystyrene (PS), styrene butadiene rubber (SBR) and different polyolefins (POs) led to the same conclusions. They reported that changing the SBR/PO dispersed phase viscosity ratio from 0.4 to 4.5 has no effect on the development of the core–shell morphology, the PO phase being systematically encapsulated by EPR as predicted by the spreading coefficient analysis.

To date, the effect of component elasticity has not been discussed with respect to composite droplet formation. Elasticity in binary immiscible blends has been predominantly studied with respect to its effect on the deformability of the dispersed phase [11–14]. Generally droplet elasticity tends to stabilize it with respect to deformation whereas matrix elasticity tends to destabilize the droplet [11,12]. In the most recent work related to binary systems, effects associated with droplet deformation in viscoelastic fluids have been observed along the vorticity axis. Levitt et al. [13] investigated the deformation of polypropylene drops of different viscosities and elasticities, sheared in a polystyrene matrix using counter-rotating parallel disks. For a highly elastic matrix, the drops of the minor phase with a diameter of about 100 μm stretch perpendicular to the shear plane. Migler [14] considered the case where the viscosity ratio of the two phases is near unity, but the elasticity ratio of the droplet to the matrix is greater than 100. He found that under conditions of weak shear and small droplets, the droplet alignment is along the shear direction, whereas for strong shear and large droplets, the alignment is along the vorticity direction.

Van Oene [15] has also considered elasticity from another point of view. In trying to describe the effect of normal stresses on droplet breakup for an extensional flowing matrix, this author developed an expression for the interfacial tension in flow by deriving a term proportional to the difference between a second normal stress function (as defined in his original paper) of the droplet and the matrix phase (Eq. (3))

$$\sigma_{dm} = \sigma_{dm}^0 + \frac{R_d}{6}(\hat{\sigma}_{2,d} - \hat{\sigma}_{2,m}) \qquad (3)$$

where σ_{dm} is the dynamic interfacial tension of a droplet of fluid d in matrix m; σ_{dm}^0, the interfacial tension in the absence of flow; R_d, the droplet diameter; $\hat{\sigma}_{2,d}$, the second normal stress function of the dispersed phase and $\hat{\sigma}_{2,m}$ is the second normal stress function of the matrix phase which depends on molecular weight, molecular weight distribution and shear stress. Note that later in this paper we will rewrite the Van Oene equation using currently accepted standard nomenclature of material functions. Van Oene's results indicate that, under conditions of dynamic flow, the elasticity differences between the phases can contribute to the interfacial tension. His work underlines that a different interfacial tension exists

under conditions of dynamic flow and that this dynamic interfacial tension can be quite different from the static one. Although there has been some disagreement concerning the precision of Eq. (3) [11], there is general agreement concerning the concept of an elastic contribution to interfacial tension.

The purpose of this study is to examine the encapsulation effects in a HDPE/PS/PMMA ternary blend system where HDPE is the matrix. The PS and PMMA viscous and elastic functions are varied over a wide range. The results will be correlated to current model predictions and a new conceptual model will be proposed.

2. Experimental procedures

2.1. Materials

HDPE, two different polystyrenes (L-PS and H-PS) and two poly(methyl methacrylate)s (L-PMMA and H-PMMA) were used in this study. A small amount (0.2 wt%) of Irganox B225 antioxidant was added to the mixture to reduce the thermal oxidation of polyethylene. Some of the characteristics of the homopolymers are summarized in Table 1.

2.2. Rheological analysis

Rheological characterization of the different polymers was carried out using a Rheometric Scientific constant stress rheometer (SR 5000). The experiments were performed in parallel-plate geometry with a diameter of 25 mm under a nitrogen atmosphere at a temperature of 200 °C. An oscillation mode of 0.1 Hz frequency was used to test the stability of the raw materials. A stress sweep was also performed to define the region of linear viscoelasticity (strain amplitude less than 4%). The dynamic mode was used to measure the complex viscosity (η^*), and the storage and loss moduli (G', G'') as a function of frequency. The frequency range of useful data for L-PMMA at 200 °C was very limited because of its low viscosity. In order to expand the range, measurements were also obtained at lower temperatures (170, 180 and 190 °C) and a master curve at 200 °C was constructed by using time-temperature superposition. This method was not necessary for the other materials. Steady shear viscosity measurements were also carried out with the same apparatus with a gap of about 1.4 mm.

2.3. Mixing

Melt mixing was carried out in a Haake Rheomix 600 batch mixer with a Haake System 90 drive. The temperature was set at 200 °C for the three heating sections. The rotation rate of the roller blades was kept constant at 50 rpm. Using an empirical calibration technique develop by Marquez et al. [16], the average

Table 1
Properties of homopolymers

Polymer	Company	Product name	M_w^a (× 10^{-3} g/mol)	M_n^a (× 10^{-3} g/mol)	Melt index[b] (ASTM, g/10 min)	Density[b] (g/cm^3) at 200 °C	η (× 10^{-3} Pa s) at 25 s^{-1} [c]	N_1 (× 10^{-3} Pa) at 25 s^{-1} [c]
HDPE	Dow	4352N	79	24	4	0.754	1.2	24
L-PS	Dow	615APR	289.8	140.9	15	0.969	1.7	110
H-PS	Polymer source	P948-St	2095.7	2681.9	–	0.969	4	1700
L-PMMA	Aldrich	20,033-6	11.9	7.8	–	1.0	0.043	0.21
H-PMMA	Rohm & Haas	IRD2	76.5	46.8	5.5	1.0[d]	7.1	530

[a] Measured by GPC.
[b] Obtained from suppliers.
[c] 25 s^{-1} represents the average shear rate in the mixer.
[d] At 230 °C.
Values for η and N_1 were obtained from Eqs. (4) and (5).

Table 2
Nomenclature and components of blends

Blend	Major phase	Minor phase (1)	Minor phase (2)
1	HDPE	L-PS	H-PMMA
2	HDPE	L-PS	L-PMMA
3	HDPE	H-PS	H-PMMA

shear rate in the mixer was estimated to about 25 s^{-1} with the HDPE matrix. Pellets or powders of the components and antioxidant were dry mixed prior to introduction into the mixer. The mass of material added to the mixer was chosen so that a constant volume of roughly 50 cm^3 was achieved for each sample, based on the density measurement at 200 °C. This corresponds to about 70% of the net volume of the mixer. At this loading, an optimum material interchange between the two chambers of the mixer is observed and there are no stagnant areas in the mixer center due to overfilling. After mixing for the required time, the mixer drive was stopped and the front plate was removed, samples were cut from the mass and dropped directly into a bath of cold water, in order to freeze-in the morphology.

The three blend systems used in this study are reported in Table 2.

2.4. Morphological analysis

2.4.1. Optical microscopy

Optical observations of polymer blend morphology of as-blended and annealed samples were made using a Nikon transmission light microscope and photomicrographs were taken with a Nikon F601$_M$ camera. Small pieces of material obtained from melt blending were cut from the mass and directly placed in a Mettler FP-82HT hot stage controlled with a Mettler FP-90 central processor. The annealing temperature was fixed at 200 °C. The polymer film thickness was typically in the order of one hundred micrometers.

2.4.2. Scanning electron microscopy

The specimens used to investigate the composite droplet morphology in the ternary blend were microtomed under liquid nitrogen to create a plane face using a microtome (Leica-Jung RM 2065) equipped with a glass knife. Samples were subjected to the appropriate chemical treatment to selectively dissolve one of the minor phases. Cyclohexane and acetic acid were used to extract PS and PMMA, respectively. After coating the desired surface with a gold–palladium alloy, the observation was carried out with a Jeol JSM 840 scanning electron microscope operated at a voltage of 10 kV.
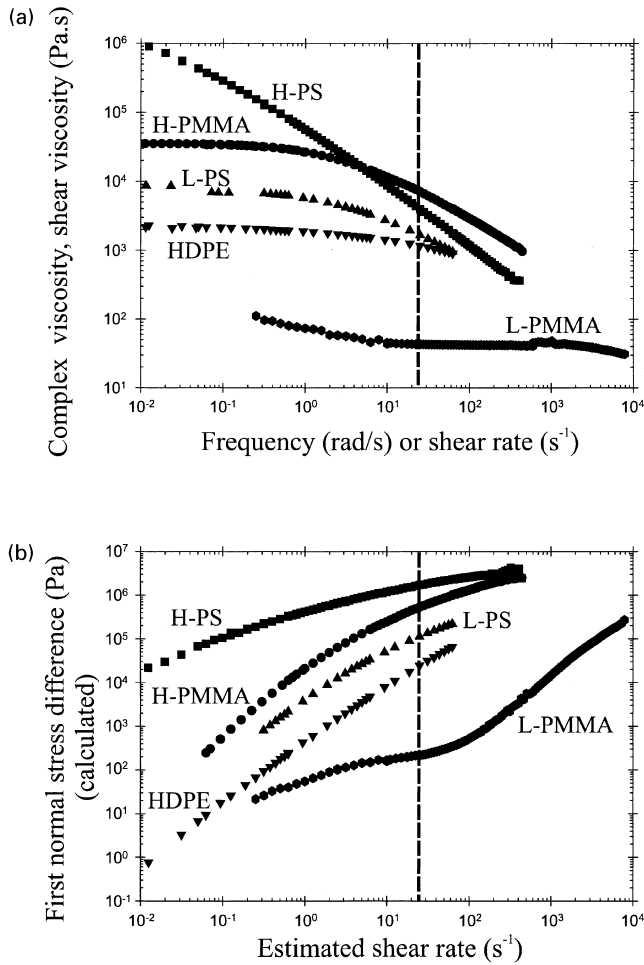
Fig. 2. Complex viscosity, shear viscosity and calculated first normal stress difference as a function of frequency or shear rate at 200 °C for the various homopolymers. The dashed line represents the average shear rate in the mixer.

3. Results

3.1. Melt viscosity and elasticity of the blend components

The steady shear viscosity and first normal stress difference of the homopolymers were estimated via Eqs. (4) and (5). The well known Cox–Merz relation [17],

$$\eta_s(\dot{\gamma}) = \frac{G''}{\omega}\sqrt{1+\left(\frac{G'}{G''}\right)^2} \qquad \text{for } \omega = \dot{\gamma} \qquad (4)$$

relates the dynamic viscosity $|\eta^*(\omega)|$ on the right-hand side of Eq. (4) to the viscosity in steady shear flow. This relation was verified for our polymers in the region of low shear rates (up to 1 s^{-1}). Laun [18] found an analogous empirical relation which relates the steady-state primary normal stress coefficient

$$\psi_1(\dot{\gamma}) = 2\frac{G'}{\omega^2}\left[1+\left(\frac{G'}{G''}\right)^2\right]^{0.7} \qquad \text{for } \omega = \dot{\gamma} \qquad (5)$$

in steady shear flow to the dynamic moduli. He demonstrated that this relation works well for many materials (linear and branched polyethylene, polypropylene, polystyrene, polyamide 6 and a PIB solution). This relation was used to estimate the first normal stress difference for the materials used in this study.

The complex viscosity as well as the viscosity and calculated first normal stress difference in steady shear flow for each of the pure melt components are plotted as functions of frequency or shear rate in Fig. 2. In the region of shear rate corresponding to the average shear rate estimated during blending (25 s^{-1}), the ranking of viscosities and first normal stress difference are $\eta_{\text{H-PMMA}} > \eta_{\text{H-PS}} > \eta_{\text{L-PS}} > \eta_{\text{HDPE}} > \eta_{\text{L-PMMA}}$ and $N_{1,\text{H-PS}} > N_{1,\text{H-PMMA}} > N_{1,\text{L-PS}} > N_{1,\text{HDPE}} > N_{1,\text{L-PMMA}}$, respectively.

At this point one needs to reflect on whether viscosity and elasticity ratios should be estimated at constant shear rate or constant shear stress. In multiphase systems, the local shear rate at the surface of a droplet under deformation may be discontinuous (although the velocity may be continuous) whereas the local shearing stress at the droplet surface may be assumed to be continuous, implying that the interface merely transmits the shearing stress from one fluid to the other. Therefore, shear stress (rather than shear rate) should be the most relevant variable for comparing viscosities and the relative strengths of the normal forces of the blend components. Since the pure materials follow the Cox–Merz relation, the shear stress is estimated as the product of the angular frequency and the measured complex viscosity. Fig. 3 shows the complex viscosity as well as the viscosity and calculated first normal stress difference in steady shear flow for the raw materials used as a function of the estimated shear stress. In the region of shear stress generated during mixing with the HDPE matrix ($\tau = 2.7 \times 10^4$ Pa), two main observations can be made upon comparing the rheological properties of the homopolymers. Firstly, the viscosity of the H-PS is greater than that of the H-PMMA. Secondly, the value of $N_{1,\text{H-PMMA}}$ is similar to that of the HDPE matrix.

Since some debate still exists concerning the use of a constant shear rate or a constant shear stress in the comparison of the rheological characteristics of multiphase systems, we will demonstrate both in this study.

Table 3
Interfacial tension for the immiscible binary systems obtained by the breaking thread method at 200 °C [19]

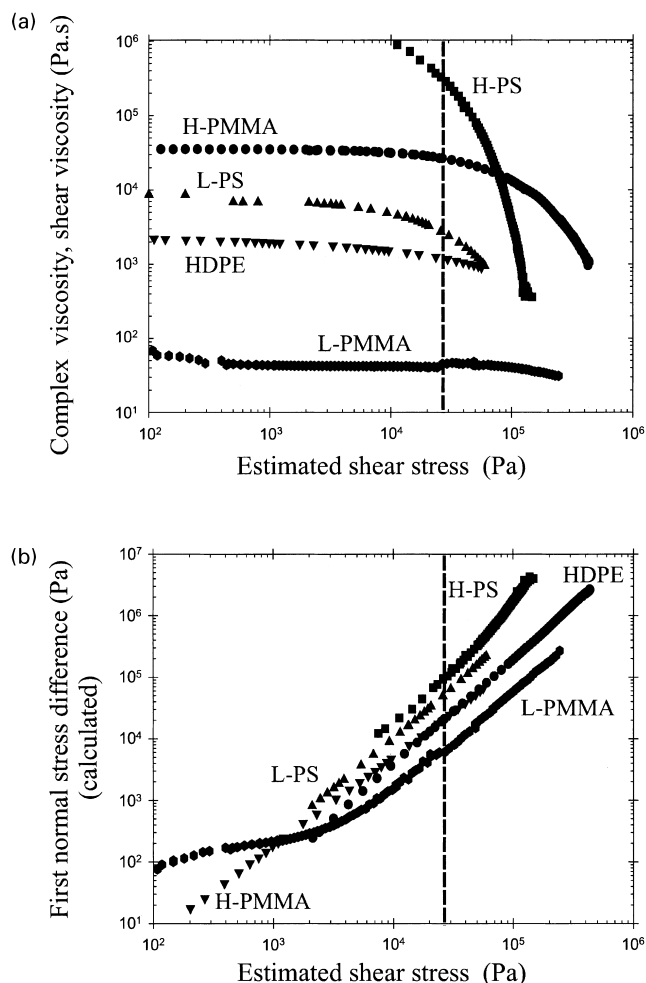| Interface (thread/matrix)	σ (mN/m)
L-PS/HDPE	5.1
H-PMMA/L-PS	2.4
H-PMMA/HDPE	8.6

Fig. 3. Complex viscosity, shear viscosity and calculated first normal stress difference as a function of the estimated shear stress at 200 °C for the various homopolymers. The dashed line represents the average shear stress in the mixer.

3.2. Interfacial tensions and spreading coefficients of the blend components

The interfacial tension data for the blend 1 components are listed in Table 3 and were measured by the breaking thread method at 200 °C. More detail on these data were reported in a previous paper [19]. Table 1 indicates that the molecular weights of the two PS and two PMMA polymers are quite different. It will be demonstrated below that these differences should not have a significant effect on the static interfacial tension values.

Only a few studies have been reported in the literature regarding the effect of molecular weight on interfacial tension between polymers for a large range of molecular weights [20–22]. In all cases the experimental data suggest that the interfacial tension first increases as a function of the molecular weight of one of the components and that the influence of molecular weight decreases significantly when the molecular weight of that polymer exceeds the value at which entanglements
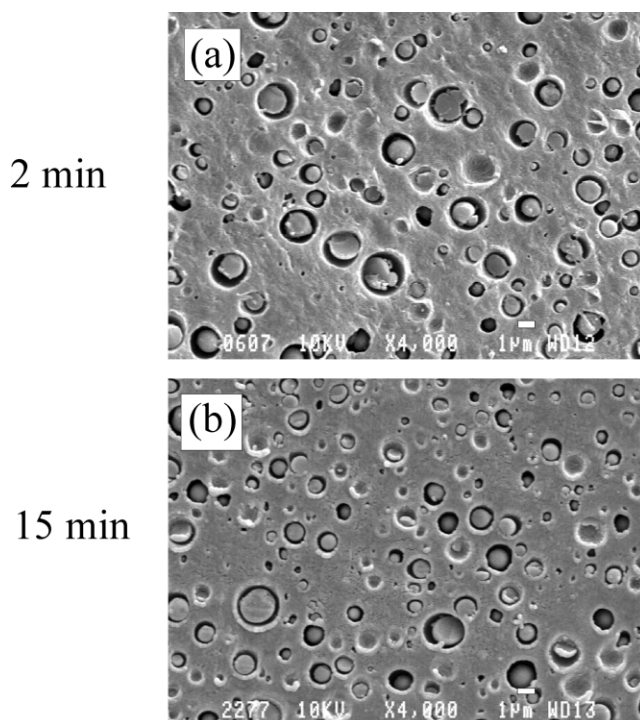

Fig. 4. SEM photomicrographs of blend 2 (L-PS/L-PMMA) at 2 and 15 min of mixing time. PS is extracted by cyclohexane. A stable composite droplet morphology is obtained within 2 min of mixing. The white bar denotes 1 μm.

occurs. Fetters et al. [23] report on data of the molecular weight between entanglements (M_e) for a number of polymers. For PS, $M_e \cong 15\,000$ g/mol at 200 °C, which is well above the molecular weight of L-PS and H-PS, whereas in the case of PMMA, $M_e \cong 12\,000$ g/mol which is close to the molecular weight of L-PMMA. As a consequence, the interfacial tension between the different pairs used in this study can be considered as constant with respect to the molecular weight.

3.3. Blend morphology

Blends were prepared with different PS and PMMA molecular weights. As reported in a previous study [19], the morphology of blend 1 (L-PS/H-PMMA) consists of an HDPE matrix and a composite droplet dispersed phase composed of a PS encapsulating phase, and PMMA subinclusions within the PS (not shown). The composite droplet morphology is achieved within 2 min of mixing. Fig. 4 (a) and (b) show the morphology for blend 2 (L-PS/L-PMMA) after extraction of the PS phase at a mixing time of 2 and 15 min, respectively. That system shows an encapsulation of PMMA particles by a PS shell. Significantly changing the PMMA core molecular weight (as compared to blend 1) has no effect on the extent, or the kinetics, of composite droplet formation. All the PMMA is located as subinclusions in the PS dispersed phase within 2 min of mixing. The analysis of the extent of composite
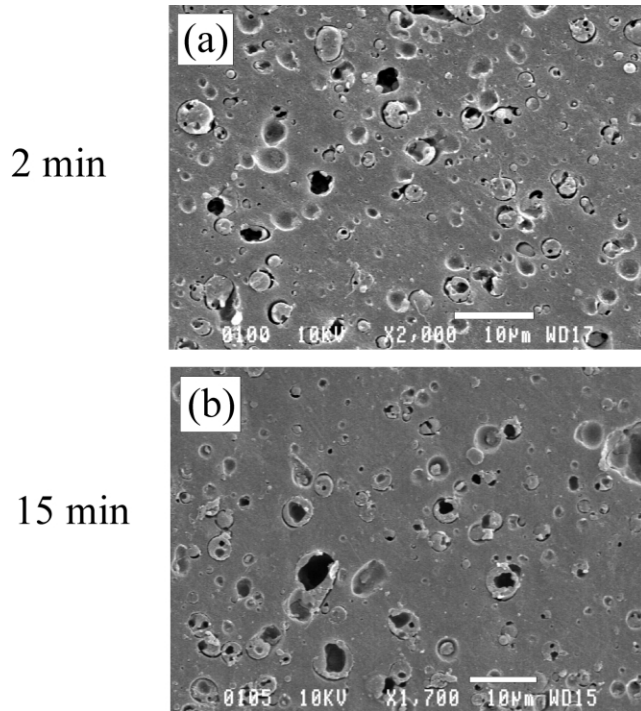
Fig. 5. SEM photomicrographs of blend 3 (H-PS/H-PMMA) at 2 and 15 min of mixing time. PS is extracted by cyclohexane. As mixing time progresses a more complete encapsulation of PS by PMMA is observed. The white bar denotes 10 μm.
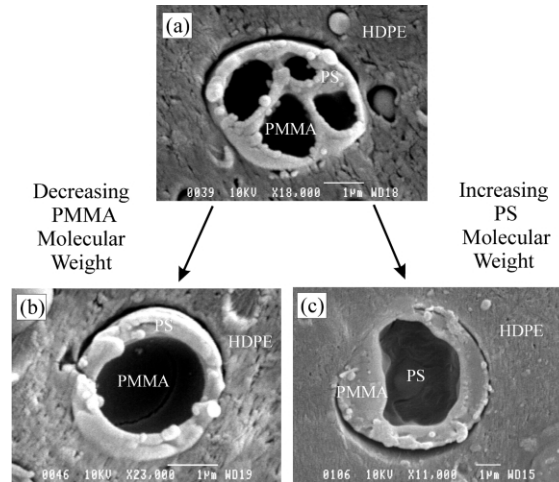

Fig. 6. Dependence of the composite dispersed morphology on PS and PMMA molecular weights. SEM photomicrographs of (a) Blend 1 (L-PS/H-PMMA); PMMA is extracted by acetic acid; PS encapsulates PMMA; (b) Blend 2 (L-PS/L-PMMA); PMMA is extracted by acetic acid; PS encapsulates PMMA; (c) Blend 3 (H-PS/H-PMMA); PS is extracted by cyclohexane; PMMA encapsulates PS. In all cases HDPE is the matrix. The white bar denotes 1 μm.

droplet formation for blends 1 and 2 was based on more than six fields of view and was quantified following a procedure reported previously [19]. It is estimated that 100% of the PMMA is present as subinclusions in the PS dispersed phase for blends 1 and 2 at all mixing times.

Blend 3 (H-PS/H-PMMA), demonstrates a clear inversion of the composite droplet structure as compared to blends 1 and 2. SEM micrographs of blend 3 shown in Fig. 5 reveal that the morphology evolves during melt mixing from a partial encapsulation of PMMA domains by PS particles (Fig. 5(a), 2 min mixing) to virtually complete encapsulation of PS particles by a PMMA shell (Fig. 5(b), 15 min mixing). No differences in structure were observed after 15 min of mixing indicating that the system achieved dynamic equilibrium.

The equilibrium morphologies obtained for blends 1–3 are shown in Fig. 6. The results clearly show that in blends 1 and 2, PS encapsulates PMMA and in blend 3 the PMMA encapsulates PS.

3.4. Annealing effects under quiescent conditions

Is the inversion in the structure of blend 3 demonstrated above due to arguments based on the relative deformability of the phases or is it due to surface free energy considerations? To examine this point, a thin film of each blend from above was examined by annealing at 200 °C. By definition, a time of annealing corresponds to

the time between the start of microscopic observations after the compression molding stage and the time when the picture was taken. The annealing process for blend 1 was reported in a previous study [19]. That work demonstrated that 90 min of annealing results in a complete transition from dispersed PMMA subinclusion particles within a given PS shell to a PMMA–PS core–shell structure. The dispersed subinclusion particles coalesced to form a perfect core structure. Composite droplets clearly experience a dual coalescence process, firstly between PMMA subinclusions within composite droplets, and secondly between composite droplets themselves. A similar process of coarsening (not shown) is observed for blend 2.

Fig. 7 (a) and (b) show the blend 3 morphology observed at 5 and 360 min of annealing, respectively. At 5 min annealing, the presence of the composite multiphase morphology is clearly observed in Fig. 7(a) and the predominant phase morphology observed for the two minor components is one of PS subinclusions dispersed in PMMA domains as one would expect from the mixing experiments. Remarkably, however, Fig. 7(b) demonstrates a core/shell inversion with time of annealing: PS subinclusions migrated to the HDPE/ PMMA interface and PMMA domains are now partly encapsulated by PS particles.

The observed reversal of the core/shell morphology for blend 3 during annealing clearly demonstrates that interfacial energy considerations dominate over viscous effects under these quiescent conditions. The structure observed is exactly that predicted by the static interfacial energy Eq. (2).
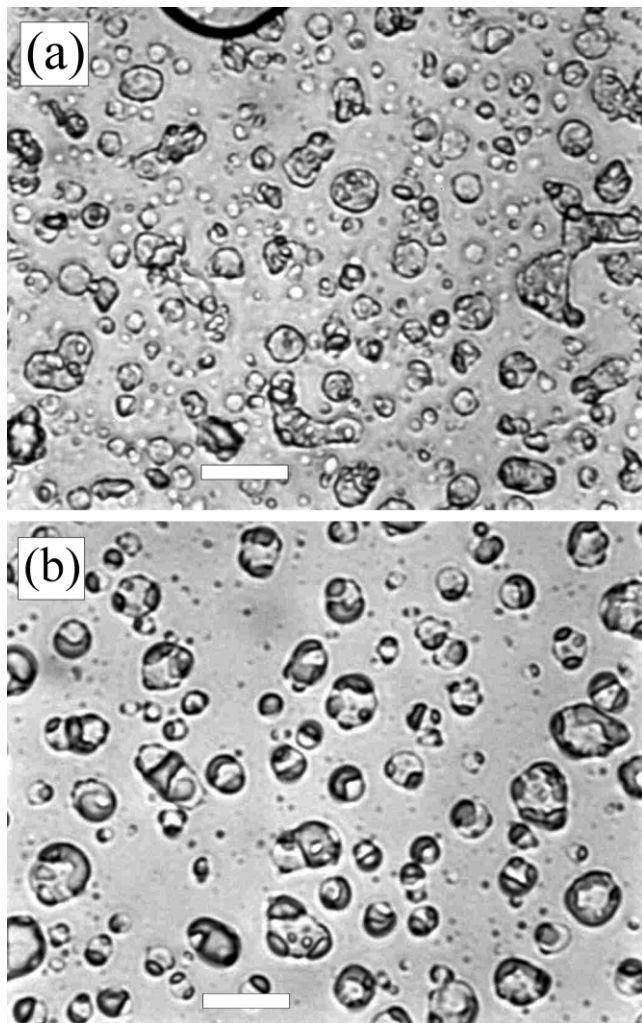
Fig. 7. Optical photomicrographs of blend 3 (H-PS/H-PMMA) at (a) 5 min and (b) 360 min of annealing time. As annealing time progresses, migration of PS droplet subinclusions to the HDPE/PMMA interface is observed. The white bar denotes 20 μm.

4. Discussion

In this part we will compare the observed morphologies to various interfacial and viscous model interpretations.

4.1. Static interfacial tension models

Section 3 demonstrates that during mixing, blends 1 and 2 form a composite droplet morphology where PS encapsulates PMMA. Blend 3 also forms a composite droplet structure, however, in that case PMMA clearly encapsulates the PS phase. Time of mixing studies indicate that all of the above structures are in dynamic equilibrium. The subsequent annealing of blend 3 demonstrates a reversal to a composite droplet morphology where PS encapsulates PMMA. In this part of the work, the equilibrium morphologies observed in Fig. 6 will be compared to the predicted morphologies based on the lowest free energy state. According to Guo et al. [5], the

interfacial free energies of the system for the different phase structures shown in Fig. 1 can be calculated by using the following equations

$$\left(\sum A_i \sigma_{ij}\right)_{\text{PS/PMMA}} = 4\pi R_e^2 \sigma_{\text{PS/PE}}^0 + 4\pi R_i^2 \sigma_{\text{PMMA/PS}}^0 \qquad (6)$$

$$\left(\sum A_i \sigma_{ij}\right)_{\text{PMMA/PS}} = 4\pi R_e^2 \sigma_{\text{PMMA/PE}}^0 + 4\pi R_i^2 \sigma_{\text{PMMA/PS}}^0 \qquad (7)$$

$$\left(\sum A_i \sigma_{ij}\right)_{\text{PS+PMMA}} = 4\pi R_i^2 \sigma_{\text{PS/PE}}^0 + 4\pi R_i^2 \sigma_{\text{PMMA/PE}}^0 \qquad (8)$$
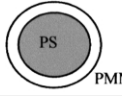
where R_e and R_i are the external and the internal radius of the composite droplet, respectively, with $R_e = \sqrt[3]{2} R_i$. Note that it is assumed here that the three different possible structures (Fig. 1) are at a constant volume of dispersed phase, and thus the $\sum n_i \mu_i$ terms in Eq. (2) are the same and can be neglected. It is also assumed for simplification that the number of particles of the dispersed phases is the same for each structure. In this calculation, R_i is arbitrarily chosen as 1 μm but changing that value has virtually no effect on the predicted morphologies. The static interfacial tension data used here are those obtained previously by the breaking thread method, and are listed in Table 3.

As mentioned earlier, three dispersed phase structures are conceptually possible for HDPE/PS/PMMA ternary blends—structure A: a composite droplet where PS encapsulates PMMA; structure B: a composite droplet where PMMA encapsulates PS and structure C: separately dispersed particles of PS and PMMA. In all these experiments, only structures A and B were observed. Furthermore, although it is possible to compare structures A and B at both constant volume and constant surface, it is impossible to do so for structure C, the separately dispersed droplets. Since Eqs. (6)–(8) are calculated at constant volume, structure C will always have a lower interfacial area as compared to A and B. For these reasons, in Table 4 we compare only the model predictions for morphologies A and B. The interfacial free energies, as estimated from Eqs. (6) and (7) result in values of 1.3×10^{-13} N m/particle and 2×10^{-13} N m/particle for structures A and B, respectively (Table 4). Therefore, it is predicted that the PS phase should encapsulate the PMMA phase in all cases. However, it can be seen from Fig. 6 that the morphology observed for the blend 3 demonstrates an opposite encapsulation behavior from that predicted by the static interfacial tension model. Since the static interfacial tensions for the various polymer pairs are identical for all three blends, neither the modified Harkins equation (Eq. (1)) or the interfacial free energy model of Guo (Eq. (2)) are able to predict the encapsulation of PMMA about PS observed for blend 3 under any conditions. How can this discrepancy be explained?

4.2. The role of the dispersed phase viscosity ratio on composite droplet formation

In this part, the influence of the dispersed phase viscosity ratio as well as the effect of the absolute viscosity of the

Table 4
Calculated values of static and dynamic interfacial free energies and dispersed phase viscosity ratio for blends 1–3

	Blend		
	1	2	3
Static interfacial energy $E = \sum A_i \sigma_{ij}^0 \times 10^{13}$ (N m/particle)	**A** (1.3) < **B** (2)	**A** (1.3) < **B** (2)	**A** (1.3) < **B** (2)
Dispersed phase viscosity ratio, η_{PS}/η_{PMMA}			
$\dot{\gamma} = cte^{a}$	0.24	39.5	0.56
$\tau = cte^{b}$	0.1	57.8	11.9
Absolute viscosity, η ($\times 10^{-3}$Pa s)			
$\dot{\gamma} = cte^{a}$ PS	1.7	1.7	4
PMMA	7.1	0.043	7.1
$\tau = cte^{b}$ PS	2.6	2.6	310
PMMA	26	0.045	26
Dynamic interfacial energy, $E = \sum A_i \sigma_{ij}$ ($\times 10^{13}$N m/particle)			
$\dot{\gamma} = cte^{a}$	**A** (14) < **B** (23)	**B** (3 3) < **A** (4.6)	**B** (47) < **A** (71)
$\tau = cte^{b}$	**A** (2.2) < **B** (2.6)	**A** (2.2) < **B** (2.3)	**B** (3.6) < **A** (4.2)
Observed morphology[c]	**A**	**A**	**B**

The predicted structure for the interfacial energy models is shown in bold. The observed morphologies are reported for comparison purposes. Structure A refers to the case of PS encapsulating PMMA in the composite droplet and structure B to PMMA encapsulating PS.

[a] Average shear rate during blending: $\dot{\gamma} = 25$ s^{-1}.

[b] Average shear stress during blending: $\tau = 2.7 \times 10^4$ Pa.

[c] In all cases HDPE is the matrix phase.

shell component, on encapsulation will be discussed in detail.

Nemirovski et al. [7] reported for a PP/LCP/PS ternary blend that the PS shell/LCP core morphology predicted by the spreading coefficient analysis is delayed. They found that an evolution of the dispersed phase morphology, from LCP particles with a low surface coverage of the more viscous PS (in a polypropylene matrix) to a complete engulfing of LCP domains by the PS took place with increasing mixing time, despite the larger PS/LCP spreading coefficient ($\lambda_{PS/LCP} = 2.59$).

In Fig. 4 and Table 4 it can be seen that blend 2 clearly demonstrates an encapsulation effect in agreement with that predicted by the interfacial energy model based on static interfacial tension (Eqs. (6)–(8)). Furthermore this morphology is observed within 2 min of mixing. The high L-PS/ L-PMMA viscosity ratio of 40 (based on constant shear rate) to 58 (based on constant shear stress)—far greater than 1— neither delays nor hinders the formation of the predicted morphology based on the model of minimization of surface free energy using static interfacial tension. These results confirm the work of Hemmati et al. [9] and Luzinov et al. [10].

The development of a composite droplet morphology where PMMA encapsulates PS in blend 3, however, is time dependent (Fig. 5). This is probably due to the high H-PS viscosity rather than a high H-PS/H-PMMA dispersed phase viscosity ratio, since as discussed above, an extreme variation in the shell/core viscosity ratio does not result in any changes in core/shell encapsulation for blend 2. The time-dependent effect could be explained by the need for a long intensive mixing period to shear off material from the highly viscous H-PS particles.

An argument based on the absolute viscosity of the phases could also be used as a potential explanation for H-PMMA encapsulating H-PS in blend 3. Since H-PS is so viscous, it could be incapable of encapsulating H-PMMA. The time-dependence results shown in Fig. 5, however, unambiguously demonstrate that the dynamic equilibrium morphology for blend 3 is a composite droplet where PMMA encapsulates PS. As the time of mixing is increased, there is a much more complete encapsulation of PMMA about PS. If the high viscosity of the PS was hindering its capability to encapsulate PMMA then the opposite effect would have been observed with time of mixing.

The annealing experiment for blend 3 under quiescent conditions reported in Section 3 is also very informative. Fig. 7 indicates for blend 3 that an inversion of the encapsulating material occurs and that the most stable morphology after annealing is clearly that of PS encapsulating PMMA. The PS particles are clearly shown to migrate to the HDPE/PMMA interface despite the difficult conditions of a high PMMA viscosity and the low PS/PMMA interfacial tension.

Cheng et al. [24] reported on the morphological study of ternary systems where one of the components is composed

of rigid non-deformable particles. Such a study is interesting in the current context since a rigid sphere can be taken as the case of infinitely high viscosity. The rigid dispersed spheres were composed of highly crosslinked methacrylated butadiene–styrene (MBS). These particles were blended with polycarbonate (PC) as the major component and polystyrene (PS) as the second minor phase. These authors showed that the rigid MBS particles become trapped at the PC–PS interface by surface forces, as predicted by a surface energy analysis model. There was no tendency whatsoever for the low viscosity PS to encapsulate the rigid MBS particles.

Considering all of the above it appears clear that interfacial energy reduction is the main driving force controlling encapsulation effects and that the viscosity ratio and the absolute viscosity have little influence on encapsulation phenomena in composite droplets.

However, the static interfacial energy prediction model fails to predict the composite droplet morphology where PMMA encapsulates PS observed for blend 3 (Table 4).

4.3. A conceptual dynamic interfacial energy model

Currently, the models developed to predict the morphology in composite droplet ternary blends have only considered the static interfacial tension. However, Van Oene has demonstrated that the interfacial tension under the conditions of dynamic flow can be quite different from the static one due to elasticity (Eq. (3)). Before looking further at the influence of elasticity on interfacial tension, it is important at this point to rewrite Van Oene's equation using more current official nomenclature for material functions describing the response of a viscoelastic fluid to shearing [25].

For a material flowing in the z direction while the velocity varies in the r direction and θ is the direction normal to the plane $\langle rz \rangle$, the current official nomenclature for the normal stress functions can be defined as follows

$$N_1 = \sigma_{zz} - \sigma_{rr} \tag{9}$$

$$N_2 = \sigma_{rr} - \sigma_{\theta\theta} \tag{10}$$

where N_1 is the first normal stress function; N_2, the second normal stress function and σ is the shear stress.

If we compare these equations with the ones proposed by Van Oene in his paper [15]

$$\hat{\sigma}_1 = T\langle rr \rangle - T\langle \theta\theta \rangle \tag{11}$$

$$\hat{\sigma}_2 = T\langle zz \rangle - T\langle \theta\theta \rangle \tag{12}$$

with $\hat{\sigma}$ the normal stress functions and T the shear stress, we can see that what Van Oene calls his first normal stress function is in fact the second normal stress function according to the current official nomenclature [25], and that his second normal stress function is a combination of the first and second normal stress functions.

Using the Weissenberg hypothesis, also cited by Van Oene [15, Eq. (4)]:

$$\sigma_{rr} = \sigma_{\theta\theta} \tag{13}$$

Van Oene's second normal stress function becomes equivalent to the current definition of first normal stress function. We can thus rewrite Van Oene's equation according to currently accepted nomenclature as follows:

$$\sigma_{dm} = \sigma_{dm}^0 + \frac{R_d}{6}(N_{1,d} - N_{1,m}) \tag{14}$$

In this form, one can see that the Van Oene equation qualitatively shows that when the difference in the first normal stress difference of the droplet phase and the matrix is positive, the elasticity acts under shear conditions as an additional interfacial tension. In the opposite case, when the elasticity of the droplet phase is smaller than that of the matrix, the interfacial tension is reduced under shear.

The influence of elasticity on composite droplet formation will be considered in this paper by introducing a dynamic interfacial tension term taken from the Van Oene equation (Eq. (14)) in the surface energy model developed by Guo et al. [5]. Eqs. (6)–(8) become

$$\left(\sum A_i \sigma_{ij}\right)_{\text{PS/PMMA}} = 4\pi R_e^2 \left[\sigma_{\text{PS/PE}}^0 + \frac{R_e}{6}(N_{1,\text{PS}} - N_{1,\text{PE}}) \right]$$
$$+ 4\pi R_i^2 \left[\sigma_{\text{PMMA/PS}}^0 + \frac{R_i}{6}(N_{1,\text{PMMA}} - N_{1,\text{PS}}) \right] \tag{15}$$

$$\left(\sum A_i \sigma_{ij}\right)_{\text{PMMA/PS}}$$
$$= 4\pi R_e^2 \left[\sigma_{\text{PMMA/PE}}^0 + \frac{R_e}{6}(N_{1,\text{PMMA}} - N_{1,\text{PE}}) \right]$$
$$+ 4\pi R_i^2 \left[\sigma_{\text{PS/PMMA}}^0 + \frac{R_i}{6}(N_{1,\text{PS}} - N_{1,\text{PMMA}}) \right] \tag{16}$$

$$\left(\sum A_i \sigma_{ij}\right)_{\text{PS+PMMA}} = 4\pi R_i^2 \left[\sigma_{\text{PS/PE}}^0 + \frac{R_i}{6}(N_{1,\text{PS}} - N_{1,\text{PE}}) \right]$$
$$+ 4\pi R_i^2 \left[\sigma_{\text{PMMA/PE}}^0 + \frac{R_i}{6}(N_{1,\text{PMMA}} - N_{1,\text{PE}}) \right] \tag{17}$$

It needs to be underlined that the major difficulty with dynamic interfacial tension is the lack of an accurate theory for its estimation. This approach is used here to indicate the tendencies that would be predicted from a consideration of elastic effects, but should not at this point be considered as a detailed model prediction.

The estimated values of the dynamic interfacial energies of blends 1–3 for phase structures A and B are calculated by using Eqs. (15) and (16) and are shown in Table 4 at a constant shear rate and stress. Negative values of the dynamic interfacial tension were taken as zero to be consistent with thermodynamic considerations. No significant changes between the predicted morphologies using a constant shear rate or a constant shear stress approach is observed, except in the case of blend 2. One should note that

the range of values of N_1 at a given shear stress are reduced compared to those observed at the corresponding shear rate, and thus this tends to reduce the effect of the dynamic part of the interfacial tension.

Considering all of the above, the preferred structure (A or B in Fig. 1) according to the different model predictions for each of the three blend systems is shown in bold characters in Table 4. The dynamic interfacial energy analysis predicts the engulfing of PMMA by PS for blend 1, as was predicted by the static interfacial energy analysis. The dynamic interfacial analysis also predicts that PMMA will encapsulate PS in blend 3. For blend 2, depending on the use of a constant shear rate or a constant shear stress, the dynamic interfacial energy approach predicts encapsulation of the PS by PMMA or encapsulation of the PMMA by PS, respectively. The use of the constant shear stress for the elasticity values results in encapsulation predictions, which correlate with the observed morphologies for all three blend systems.

The results presented here strongly indicate that encapsulation phenomena in composite droplets is dominated by surface free energy considerations and that the dynamic interfacial tension needs to be taken into account. There is also a clear need for a more refined development of the relationship of dynamic interfacial tension to component elasticity.

5. Conclusion

This study examines the influence of the molecular weight of the dispersed phase components on encapsulation effects in the composite droplet phase for a ternary blend composed of PS and PMMA dispersed in HDPE. Three different blends were prepared and the results clearly show that depending on the molecular weight of the PS and PMMA, PS could be made to encapsulate PMMA (blends 1 and 2) and PMMA could also be made to encapsulate PS (blend 3). Time of mixing experiments indicate that all three of the above structures attain dynamic equilibrium during melt mixing.

Arguments based on the effect of viscosity ratio or the absolute viscosity of the phases do not explain the above results. Furthermore, when the PMMA shell/PS core structure from blend 3 was subjected to static annealing at high temperature, the PS core is shown to migrate to the shell position. This reversal of the core/shell phases during annealing is a clear proof that interfacial energy considerations dominate over viscous forces in composite droplet formation. However, the well-known predictive models for encapsulation in composite droplets, based on the estimation of spreading coefficients from static interfacial tension or the estimation of static interfacial free energy, can under no conditions predict the encapsulation of PMMA around PS in a HDPE matrix. Since the interfacial tension between components in dynamic flow can be quite different from the static interfacial tension, a modified interfacial energy equation, incorporating the Van Oene estimation of dynamic interfacial tension, was developed as a conceptual model. It is found that this approach is able to reasonably explain the encapsulation behavior observed for the three blend systems.

References

[1] Torza S, Mason SG. J Colloid Sci 1970;33(1):67–83.
[2] Favis BD, Chalifoux JP. Polymer 1988;29:1761–7.
[3] Favis BD, Lavalée C, Derdouri A. J Mater Sci 1992;27:4218.
[4] Hobbs SY, Dekkers MEJ, Watkins WH. J Mater Sci 1988;23: 1598–602.
[5] Guo HF, Packirisamy S, Gvozdic NV, Meier DJ. Polymer 1997;38: 785–94.
[6] Legros A, Favis BD, Carreau P, Michel A. Polymer 1997;38:5085–9.
[7] Nemirovski N, Siegmann A, Narkis M. J Macromol Sci, Phys 1995; B34(4):459–75.
[8] Gupta AK, Srinivasan KR. J Appl Polym Sci 1993;47:167–84.
[9] Hemmati M, Nazokdast H, Panahi HS. J Polym Sci 2001;82: 1129–37.
[10] Luzinov I, Pagnoulle C, Jérôme R. Polymer 2000;41:7099–109.
[11] Elmendorp JJ, Maalcke RJ. Polym Engng Sci 1985;25(16):1041–7.
[12] Ghodgaonkar PG, Sundararaj U. Polym Engng Sci 1996;36:1656–65.
[13] Levitt L, Macosko C, Pearson S. Polym Engng Sci 1996;12:1647–55.
[14] Migler KB. J Rheol 2000;44(2):277–90.
[15] Van Oene H. J Colloid Interf Sci 1972;40:448–67.
[16] Marquez L, Quijano J, Gaulin M. Polym Engng Sci 1996;36: 2556–63.
[17] Cox WP, Merz EH. J Polym Sci 1958;28:619–22.
[18] Laun HM. J Rheol 1986;30(3):459–501.
[19] Reignier J, Favis BD. Macromolecules 2000;33:6998–7008.
[20] Arashiro EY, Demarquette NR. J Appl Polym Sci 1999;74:2423–31.
[21] Ellingson PC, Strand DA, Cohen A, Sammler RL, Carriere CJ. Macromolecules 1994;27:1643–7.
[22] Kamal MR, Lai-Fook R, Demarquette NR. Polym Engng Sci 1994; 34(24):1834–9.
[23] Fetters LJ, Lohse DJ, Milner ST, Graessley WW. Macromolecules 1999;32:6847–51.
[24] Cheng TW, Keskkula H, Paul DR. Polymer 1991;33:1606–19.
[25] Dealy JM. J Rheol 1984;28(3):181–95.